COMPRESSIBILITY IN FUSED FILAMENT FABRICATION

D.O. Kazmer^{1,*}, A. Colon¹, T. Coogan^{1,2}, A. Mubasshir¹, A. Peterson¹

Department of Plastics Engineering, Univ. Mass. Lowell, Lowell, Massachusetts

² Saint-Gobain Research North America, Northboro, Massachusetts

Abstract

Fused filament fabrication (FFF) is one of the most accessible and flexible additive manufacturing processes. However, it is plagued by consistency issues related to material deposition. The role of compressibility is explored with an instrumented nozzle to relate the observed printing pressure to variations in deposited road widths. Variations in road width are analyzed relative to those predicted using a double domain Tait equation (PVT model) for high impact polystyrene (HIPS). Compressibility was found a critical effect, varying the road widths by up to 50% when accelerating and decelerating. The effect of the speed of transient stress propagation was also investigated but found insignificant.

Introduction

Fused filament fabrication (FFF), also known as fused deposition modeling (FDM®), is a 3D printing technique that deposits roads of molten polymer that solidify into the final, desired shape. FFF enables the creation of complex designs without tooling that are difficult to produce or otherwise unattainable via traditional manufacturing. Despite the benefits and widespread use of FFF, dominating constraints in application may include limited part strength, high degree of anisotropy, poor print resolution, inadequate surface finish, lack of repeatability, uncontrolled shrinkage and warpage, limited process observability and quality assurance, low production rates, and others.

Many of these limitations can be compensated by printing at higher resolutions with improved printing speed and consistency. While print resolution is widely believed to be primarily a function of the machine design, e.g. the stepper motor and gearing, it is increasingly understood that the material plays a critical role in the classic triad of material:processing:property interaction. Significant work has focused on the role of polymer viscosity and molecular diffusion, for example, to predict void content and part strength.

This paper solely focuses on the role of polymer compressibility with respect to variation in the output volumetric flow rate and resulting printed road width. The reason is that the observed road width is directly related to surface finish, bond width, and void fraction. By understanding and compensating for compressibility effects, the print quality can be better controlled across varying print speeds.

Experimental

Experiments were conducted on a Lulzbot Taz6 printer augmented with an instrumented nozzle shown in Figure 1. The nozzle has a 0.53 mm diameter orifice with a land length of 1.6 mm. A 2.38 mm side bore was reamed to provide access for a load column provided with an intrusive thermocouple. The load column was supported by a 44.5 N load cell, which allowed the measurement of force and close estimation of the exerted melt pressure; details pertaining to calibration and validation as well as the supervisory control system are available [1, 2].

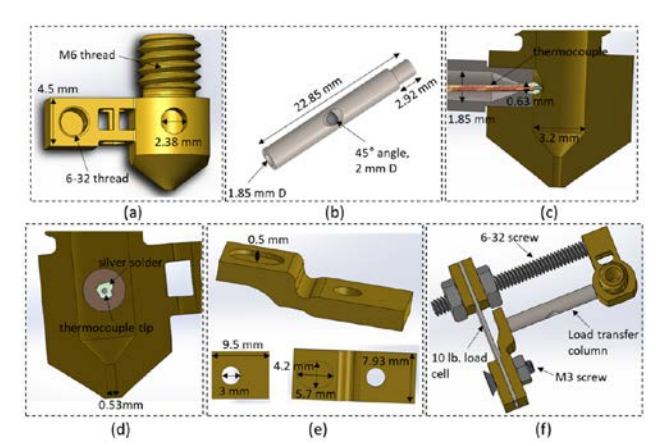


Figure 1: In-line rheometer nozzle design: (a) custom nozzle, (b) load transfer column, [(c) and (d)] load transfer column plus thermocouple inserted into the nozzle pressure port, (e) custom clamps for the load cell, and (f) full assembly.

The described apparatus has been used to monitor the viscosity and contact pressure of high impact polystyrene (HIPS). The same spool of feedstock material in [2], HIPS Natural from eSun (Shenzhen, China), was used in this study. To examine the effect of printing parameters on volumetric flow rate and road width, a full factorial design of experiments (DOE) was implemented with three factors at three levels. The three factors (and levels) were:

- Layer height, H (0.10, 0.25, and 0.40 mm);
- Road width, W (0.35, 0.50, and 0.65 mm); and,
- Print speed, S (1000, 2500, and 4000 mm/minute).

The bed and nozzle temperature were set to their central values for processing HIPS, equal to 80 and 250 °C, respectively. The implemented DOE is provided in Table 1. To avoid excessive nozzle pressures, run conditions resulting in flow rates greater than 10 mm³/s were skipped as indicated by the strikethrough font styles.

Table 1: Design of Experiments (DOE)

	Tbed	Tnoz	Н	W	S
DOE Run	[°C]	[°C]	[mm]	[mm]	[mm/s]
1	80	250	0.1	0.35	16.67
2	80	250	0.1	0.35	41.67
3	80	250	0.1	0.35	66.67
4	80	250	0.1	0.5	16.67
5	80	250	0.1	0.5	41.67
6	80	250	0.1	0.5	66.67
7	80	250	0.1	0.65	16.67
8	80	250	0.1	0.65	41.67
9	80	250	0.1	0.65	66.67
10	80	250	0.25	0.35	16.67
11	80	250	0.25	0.35	41.67
12	80	250	0.25	0.35	66.67
13	80	250	0.25	0.5	16.67
14	80	250	0.25	0.5	41.67
15	80	250	0.25	0.5	66.67
16	80	250	0.25	0.65	16.67
17	80	250	0.25	0.65	41.67
18	80	250	0.25	0.65	66.67
19	80	250	0.4	0.35	16.67
20	80	250	0.4	0.35	41.67
21	80	250	0.4	0.35	66.67
22	80	250	0.4	0.5	16.67
23	80	250	0.4	0.5	41.67
24	80	250	0.4	0.5	66.67
25	80	250	0.4	0.65	16.67
26	80	250	0.4	0.65	41.67
27	80	250	0.4	0.65	66.67

For each run of the DOE, a base layer 0.75 mm wide and 0.30 mm high was printed to minimize inaccuracies caused by the leveling process. A second layer was then printed at the conditions indicated in Table 1. As shown in Figure 2, an "out & back" print was provided consisting of:

- 1. A 5 s steady line at run conditions per Table 1;
- 2. A 2 mm deceleration to a print speed of 5 mm/s while maintaining the same layer height & road width;
- 3. A 1.06 mm transverse line at a print speed of 5 mm/s while maintaining the same layer height & road width;
- 4. A 2 mm acceleration to the set print speed while maintaining the same layer height & road width;
- 5. A 5 s steady line at run conditions per Table 1.



Figure 2: Observed prints per DOE of Table 1

The different lengths of the print pattern in Figure 2 correspond to the print velocities of 1000, 2500, and 4000 mm/minute as specified in Table 1; each out and back line corresponds to 1 DOE run with the missing lines indicating the omitted DOE runs. The red box at right in Figure 2 indicates the portion of interest during the controlled acceleration and 1.06 mm transverse line that corresponds to the detail view of Figure 3. The arrows on run 21 in Figure 3 indicate the 2 mm deceleration (red), constant

speed transverse line (orange), and the 2 mm acceleration (green). It is observed that there is significant variation in the printed road width as a function of the deceleration and acceleration. The hypothesis is that this variation is due to the change in print velocity from the faster print speeds specified per Table 1 to the slower print velocity of 300 mm/minute (5 mm/s) for the transverse line.

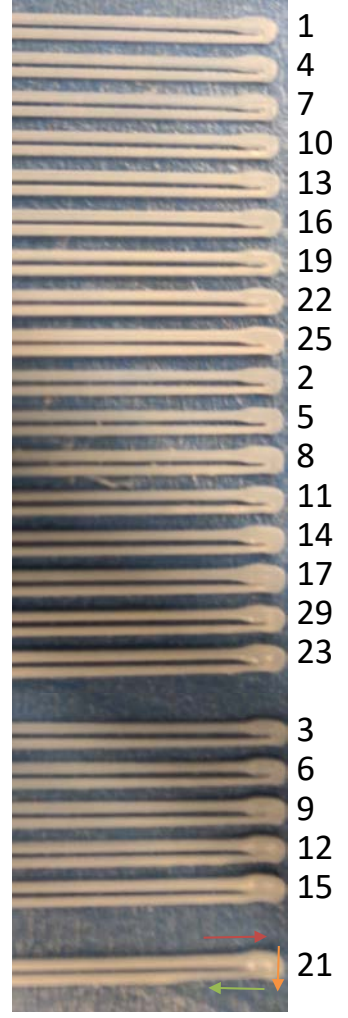


Figure 3: Detail image of transverse line

Image analysis was conducted by overlaying sight rectangles and lines on a 100 cm tall scaled image; the resolution of the fitted shapes was 0.01 mm. The widths, W, of the printed roads while decelerating and accelerating adjacent the transverse lines were measured and are provided in Table 2. The approximate distance of the transient portion, dX, when decelerating and then accelerating from the print speeds specified in Table 1 were also measured to show the duration of the effect of compressibility within the 2 mm span. The calculated volumetric flow rate and observed dimensional results are provided in Table 2. It is observed for every run condition that the width in the decelerating portion is wider than the road width set per Table 1, while the width in the accelerating portion is narrower.

Table 2: Caclulated flow rates and measured widths per DOE

	Q	Deceleration		Acceleration	
DOE Run	[mm^3/s]	dX [mm]	W [mm]	W [mm]	dX [mm]
1	0.58	0.26	0.67	0.26	0.5
2	1.46	0.51	0.65	0.28	0.49
3	2.33	0.36	0.64	0.22	0.71
4	0.83	0.28	0.67	0.31	0.4
5	2.08	0.57	0.65	0.28	0.52
6	3.33	0.38	0.66	0.23	0.48
7	1.08	0.25	0.64	0.34	0.2
8	2.71	0.56	0.72	0.29	0.48
9	4.33	0.3	0.69	0.26	0.91
10	1.46	0.25	0.64	0.33	0.44
11	3.65	0.61	0.72	0.24	0.58
12	5.83	0.53	0.77	0.2	0.75
13	2.08	0.28	0.64	0.35	0.32
14	5.21	0.54	0.79	0.24	0.53
15	8.33	0.53	0.78	0.27	0.57
16	2.71	0.35	0.68	0.35	0.62
17	6.77	0.73	0.84	0.23	0.53
18	10.83				
19	2.33	0.56	0.63	0.3	0.51
20	5.83	0.76	0.77	0.22	0.54
21	9.33	0.62	0.8	0.29	2.11
22	3.33	0.45	0.66	0.33	0.37
23	8.33	0.81	0.83	0.21	0.67
24	13.33				
25	4.33	0.48	0.71	0.34	0.39
26	10.83				
27	17.33				

The nozzle pressures were acquired at a sampling rate of 1 kHz, then down sampled to a rate of 100 Hz for analysis and storage. Figure 4 plots the dynamic nozzle pressure data across the 1800 s duration of the implemented DOE. The nozzle pressure varies not only with the DOE run settings of Table 1, but also with the printing of the base layer and nozzle repositioning between DOE runs.

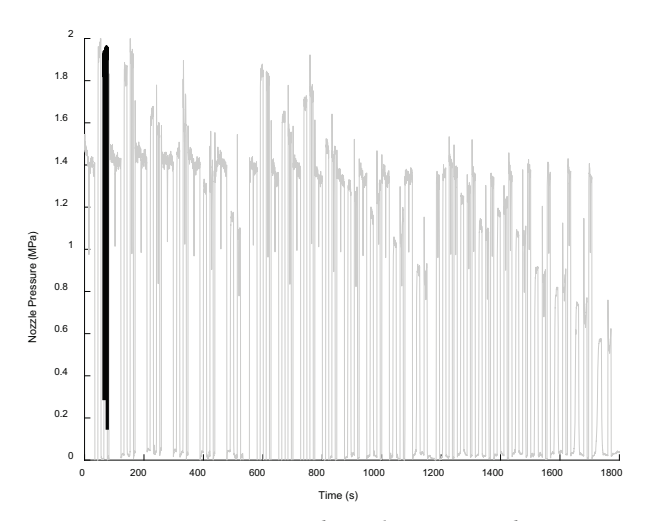


Figure 4: Acquired nozzle pressure data

Figure 5 provides a detail view of the bolded transient process data shown in Figure 4, which corresponds to run 21 of the DOE described by Table 1. It is observed that the nozzle pressure during the first and last 5 s of the trace are

quite steady, which correspond to the printing of a road 0.35 mm wide and 0.4 mm high at a print speed of 4000 mm/minute. In the middle, there is a deceleration and acceleration period during which the print speed is reduced to 300 mm/minute as described. The first dashed vertical line is the onset time of deceleration; the second line is the onset of the transverse line being printed at 300 mm/minute; the third line is the onset of acceleration; the fourth line is the end of the set acceleration. The lag between the set accelerations and the resulting transient pressure behavior suggests potentially significant compressibility in the polymer as next analyzed.

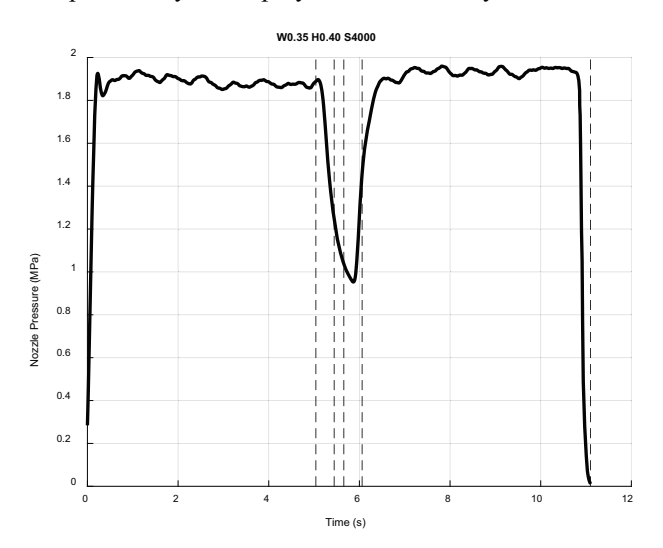


Figure 5: Transient nozzle pressure for run 21 of Table 1

Analysis

The volumetric flow of the extruded plastic is governed by the thermal expansion and compressibility of the polymer melt, both of which can be well modeled by the double domain Tait equation [3]. The term "double domain" implies that the specific volume is modeled separately in the solid and melt states as a function of pressure and temperature:

$$v(T,P) = v_0(T)\left(1 - 0.0894\ln\left(1 + \frac{P}{B(T)}\right)\right) + v_T(T,P)$$
 (1)

For temperatures below the transition temperature, the reference specific volume, $v_0(T)$, and compressibility, β , are modeled using the coefficients of Table 3 as:

$$v_0 = b_{1,s} + b_{2,s} (T - b_5)$$

$$B(T) = b_{3,s} \exp(-b_{4,s} (T - b_5))$$
(2)

These coefficients are determined by use of a pvT diagram for the given material. The coefficient b_5 is the transition temperature at zero pressure, and b_6 is the rate of change of the transition temperature with respect to pressure. where $b_{1...4,s}$ are material coefficients related to the material

properties in the solid state. For temperatures above the transition temperature, the reference specific volume and compressibility are similarly modeled albeit with a different set of coefficients. The transition temperature between the solid and melt states is modeled as a function of pressure as:

$$T_{t}(P) = b_{5} + b_{6}P \tag{3}$$

The term v_T represents the additional specific volume associated with the transition volume of semi-crystalline polymers, and is 0 for amorphous polymers such as HIPS. The modeled specific volume is plotted in Figure 6.

Table 3: Double domain Tait coefficients for PS

Coefficient	Value		
b1m (m³/kg)	9.97E-04		
b2m (m ³ /kg K)	5.98E-07		
b3m (Pa)	1.56E+08		
b4m (1/K)	4.58E-03		
b1s (m³/kg)	9.94E-04		
b2s (m³/kg K)	2.96E-07		
b3s (Pa)	1.92E+08		
b4s (1/K)	4.96E-03		
b5 (K)	394.25		
b6 (K/Pa)	8.10E-08		

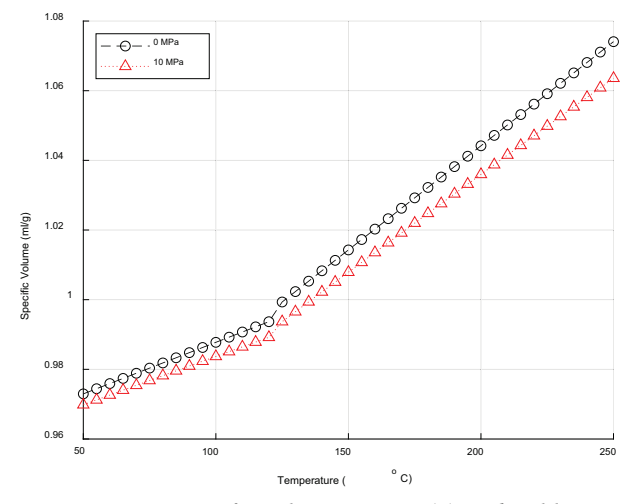


Figure 6: Specific volume per eq. (1) and Table 3

Figure 7 provides a cut-away view of a Titan hot end with a 3 mm filament diameter as compatible with the Lulzbot Taz 6. It is observed that there is a cold section at top (colored blue in Figure 7), a transition heat brake section at center (colored yellow), and the hot nozzle at the bottom (colored red). To simplify the analysis, the driven filament is modeled as a cold section with a length of 53.47 mm and a diameter of 2.85 mm and a hot section with a length of 18.45 mm and a diameter of 3.00 mm. This approximation is first order accurate given the assumption of a linear temperature profile in the heat brake.

The volumetric flow rate can then be modeled based on the programmed machine control superimposed with the volumetric source or sink based on the change in pressure. Specifically, given a filament having a cross sectional area, A, and an extrude position, E, the volumetric flow $Q_{\rm Driven}$ due to the filament driven by the spur gear is:

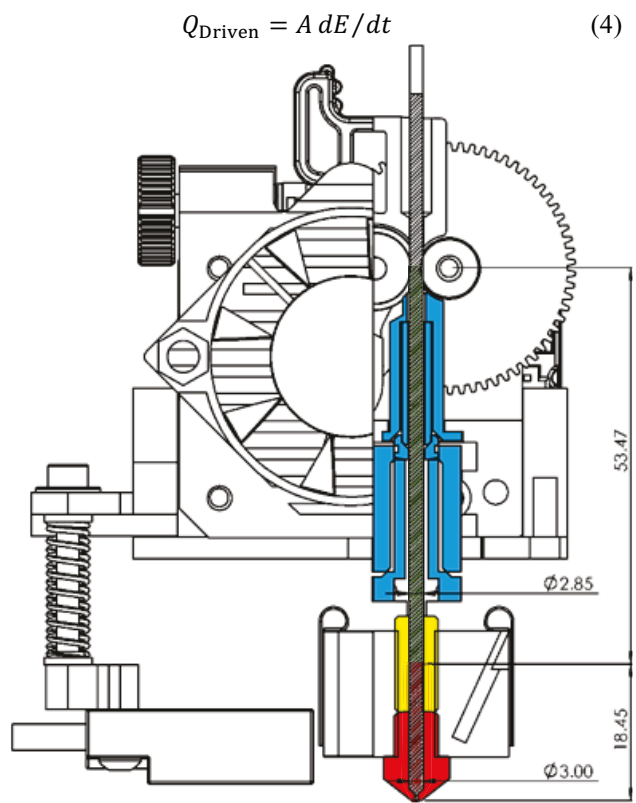


Figure 7: Cut away of Titan hot end

The volumetric flow rate due to compressibility can likewise be calculated based on the double domain Tait equation of eq. (1) and the time varying pressure, P(t), using a backward difference as:

$$Q_{\text{Compressibility}} = \sum_{i \in [\text{Cold}, \text{Hot}]} \frac{V_{i} \left(v \left(T_{i}, P(t) \right) - v \left(T_{i}, P(t - \Delta t) \right) \right)}{v \left(T_{i}, P(t) \right) \Delta t}$$
(5)

where V is the volume and v is the specific volume in the cold and hot sections as a function of pressure and temperature. Here, $T_{\rm Hot}$ and $T_{\rm Cold}$ are assumed to be 250 °C and 50 °C, respectively.

Given the output volumetric flow rate due to the driven and compressible flow, the road width, W, can be estimated as from the layer height, *H*, and print speed, *S*, as:

$$w = (Q_{\text{Driven}} + Q_{\text{Compressibility}})/(HS)$$
 (6)

Upon review of the results, it was considered that the printed road width may also be a function of the speed of sound causing a delay between the driven gear rotation and the lateral bed velocity due to the time required for the stress wave to propagate through the filament medium. The speed of sound is related to the transients because sound propagation is equivalent to the speed of energy transport for non-dispersive medium. The speed of sound, c, $i \in [Cold, Hot]$, can be estimated from the partial derivative of pressure with respect to density, ρ :

$$c = \sqrt{\left(\frac{\partial P}{\partial \rho}\right)_s} \tag{7}$$

The speed of sound can be handily estimated using equation (7) with the double domain Tait equation (1). The time delay, τ , can then be estimated by adding the delay in the cold and hot section as the length of each section divided by the speed of sound in the section:

$$\tau = \sum_{i \in [\text{Cold}, \text{Hot}]} \frac{L_i}{c_i(T_i, P(t))}$$
(8)

Results

The estimated output volumetric flow rate with and without compressibility is plotted in Figure 8 for the run conditions and transient nozzle pressure of Figure 5. It is observed that there is a significant delay in the output volumetric flow rate at the start of printing. This delay is due to the pressurization of the melt, which causes the output volumetric flow rate to lag what would otherwise be a volume proportional to the rotational velocity of the drive gear.

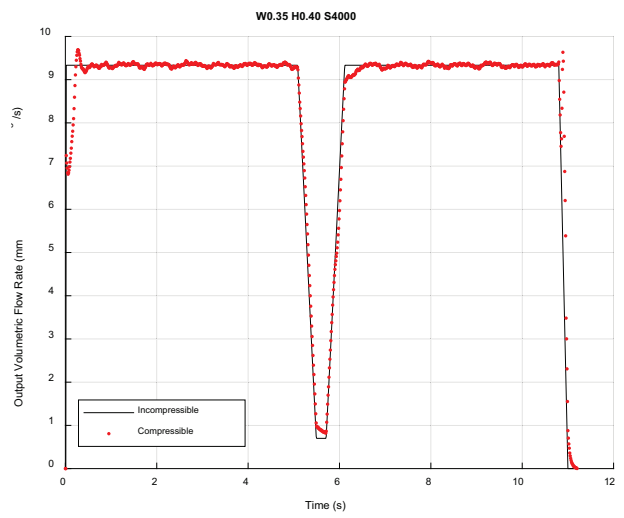


Figure 8: Output volumetric flow rates with and without compressibility

Between 5 and 6 s, the printer is decelerating to 300 mm/minute and then back up to 4000 mm/minute. Lags in

the volumetric flow rate are again observed, with the compressible flow rate always being greater than the expected incompressible flow rate until the acceleration begins. This behavior is due to the decreasing nozzle pressure (associated with the decreasing volume of material in the nozzle) such that the decompression causes more output volumetric flow than would occur with an incompressible fluid. During acceleration, the volumetric output with compressibility lags that of the incompressible fluid since the melt pressure is increasing and, as such, the melt must densify prior to extrusion. At the end of the run, the output volumetric flow rate lags as the extruder slows down and the melt ceases to flow.

Knowing the print speed velocity profile as described in the experimental section, the printed road width can be estimated according to equation (6). The resulting width predictions are plotted in Figure 9. The effect of compressibility is very significant with respect to the variation in the road width, causing the road to become wider than the planned width of 0.35 mm while the extruding and printing are slowing down. Then, the road width becomes narrower as the extruding and printing accelerate.

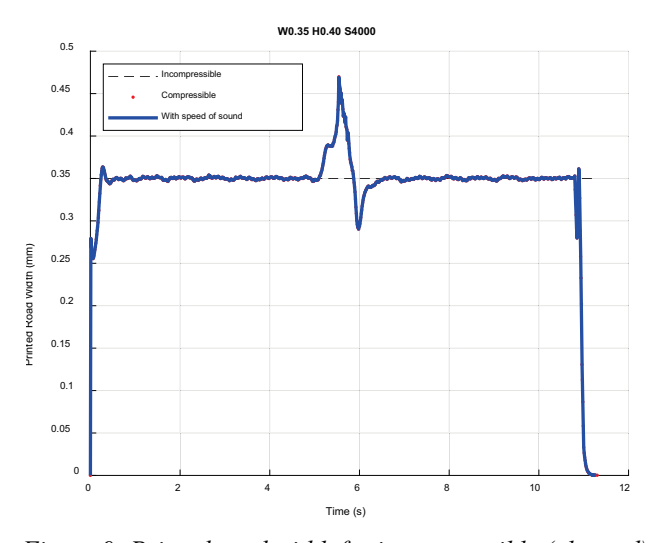


Figure 9: Printed road width for incompressible (planned) flow, compressible flow, and compressible flow including the effect of the speed of sound

The effect of the speed of sound on the printed road width is also plotted in Figure 9. The speed of sound in the hot and cold sections are estimated from the Tait equation to be 1770 and 1020 m/s, respectively. Given the lengths of their respective filament sections, the time delays in the cold and hot sections were 30 and 18 μs , providing a total delay of 48 μs . While this delay is on the order of the 40 μs sampling time given a sampling frequency of 1 kHz, it is negligible with respect to the observed process dynamics. Accordingly, the traces for the printed road width due to compressibility with and without the speed of sound effectively overlap.

The data and results of Figures 5, 8, and 9 correspond to run 21 of the DOE described by Table 1. The pressure and volumetric flow rates were inspected for all DOE runs and found to exhibit varying behaviors related to the printing pressures and speeds. The volumetric flow rates and widths resulting from compressibility were predicted and visualized with the results provided in Figure 10. It is observed that the predicted widths mimic the behaviors shown in Figure 3, which is presented to the right of the visualized results. There are some discrepancies, most likely due to the synchronization of the moving build plate with the acquired pressure. It is clear that compressibility is a major effect that must be considered to achieve precision 3D printing.

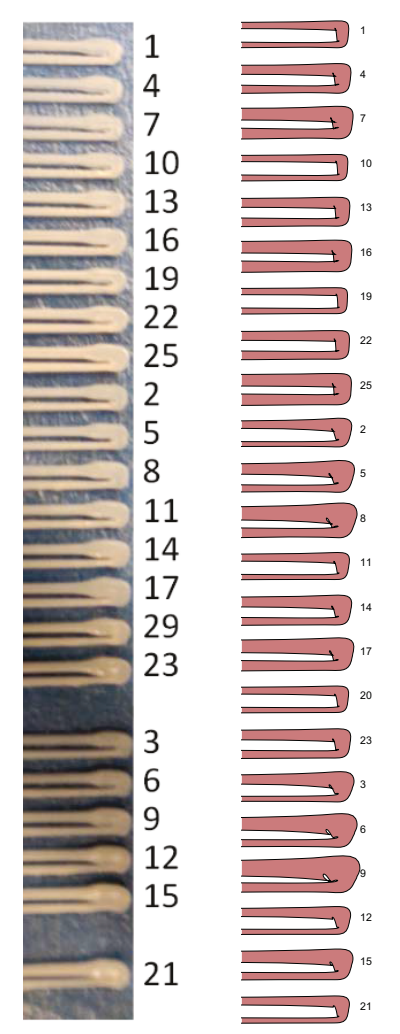


Figure 10: Visualized widths predicted from compressible flow simulation with experimental results for comparison

Discussion

The results indicate that compressibility is a major effect that must be considered to achieve precision and consistency. The machine programs for implementing the described DOE were themselves generated from Matlab scripts that provided a positioning accuracy of 10 microns. Given the small length of the transverse lines (see Figures 2 and 3) bounded by the decelerating and accelerating portions, the amount of extruded material in some cases was literally zero. In other words, the G1 command on the E axis of the extruder remained unchanged for some road widths and layer heights. The large widths of the transverse line observed in Figure 3 are thus due primarily to compressibility.

Viewing these results, it is clear that compressibility should be modeled when generating machine programs (g code) for fused filament fabrication. These programs can be improved by estimating pressure using non-Newtonian viscosity models (e.g. Cross-WLF or power law) and compensating for compressibility using the double domain Tait equation. Even generic material constitutive models would provide significant improvements in consistency.

For improved precision, instrumented printers and observed nozzle pressures can be used to estimate the effect of compressibility on flow rates. The possibility to observe and correct the effect in real time necessitates improved instrumentation including, at least, a filament position encoder and nozzle pressure transducer. The variation in the results of Figure 9 compared to the observed prints of Figure 3 are due to lack of synchronization between the acquired nozzle pressures, the filament actuation, and the build plate motion. This suggests the need to either embed the analysis within the machine controller (e.g. Marlin, etc.) or to also instrument the translational X, Y, and Z axes with position transducers or closed loop stepper motors in order to reliably observe the process with an auxiliary data acquisition system or supervisory, model-based controller.

Conclusions

Fused filament fabrication (FFF) is widely and successfully used in a variety of applications. For the most part, endusers specify conservative print settings to produce reliable prints. More advanced users are more aggressive, and advantageously apply acceleration, deceleration, and suck back to improve the quality and printing speed. Even though pressures are relatively low in fused filament fabrication, compressibility can have a significant impact on volumetric flow rates and printed road widths. Modelbased approaches based on the polymer physics can far outperform default settings based on prior experience while also enabling automatic quality assurance using improved process instrumentation.

Acknowledgements

This material is based upon work supported by the National Science Foundation under Grant No. 1914651. Any opinions, findings, and conclusions or recommendations

expressed in this material are those of the author(s) and do not necessarily reflect the views of the National Science Foundation.

References

- [1] T. J. Coogan and D. O. Kazmer, "In-line rheological monitoring of fused deposition modeling," J. o. R. vol. 63, no. 1, pp. 141-155, 2019.
- [2] T. J. Coogan and D. O. Kazmer, "Modeling of interlayer contact and contact pressure during fused filament fabrication," J. o. R. vol. 63, no. 4, pp. 655-672, 2019.
- [3] P. Zoller and D. J. Walsh, Standard Pressure-Volume-Temperature Data for Polymers. CRC Press, 1995.